Nanoscale

PAPER

View Article Online
View Journal | View Issue

Cite this: *Nanoscale*, 2024, **16**, 4900

Reversible optical control of magnetism in engineered artificial multiferroics†

Diego A. Ochoa, ‡[a] Enric Menéndez, ‡[b] Jesús López-Sánchez, [c] Adolfo Del Campo, [c] Zheng Ma, [b] Irena Spasojević, [b] Ignasi Fina, [d] José F. Fernández, [c] Fernando Rubio-Marcos, *[c] Jordi Sort *[b,e] and José E. García *[a]

Received 31st October 2023,
Accepted 30th January 2024

DOI: 10.1039/d3nr05520e

rsc.li/nanoscale

Optical means instead of electric fields may offer a new pathway for low-power and wireless control of magnetism, holding great potential to design next-generation memory and spintronic devices. Artificial multiferroic materials have shown remarkable suitability as platforms towards the optical control of magnetic properties. However, the practical use of magnetic modulation should be both stable and reversible and, particularly, it should occur at room temperature. Here we show an unprecedented reversible modulation of magnetism using low-intensity visible-light in $Fe_{75}Al_{25}/BaTiO_3$ heterostructures, at room temperature. This is enabled by the existence of highly oriented charged domain walls arranged in arrays of alternating in-plane and out-of-plane ferroelectric domains with stripe morphology. Light actuation yields a net anisotropic stress caused by ferroelectric domain switching, which leads to a 90-degree reorientation of the magnetic easy axis. Significant changes in the coercivity and squareness ratio of the hysteresis loops can be light-modulated, encouraging the development of novel low energy-consumption wireless magneto-optical devices.

Introduction

Light-induced control of magnetism is a promising technology for the implementation of novel magnetoelectronic devices because it is a non-contact actuation method that entails ultra-low power dissipation.[1–7] Unfortunately, deterministic and reversible control of magnetic properties using light has proven to be challenging and, so far, restricted to a few specific materials with still limited commercial viability.[8] For this reason, the scientific community has turned its attention to multiferroic materials which are highly appealing owing to their magnetoelastic and magnetoelectric properties.[9,10] Multiferroics allow control of magnetic properties through externally applied electric fields.[11] Since the production of electric fields is far less energy-consuming than magnetic fields, multiferroics constitute a promising technological breakthrough to write magnetic data directly with an applied voltage, thus minimizing Joule heating effects. However, single-phase multiferroics exhibiting intrinsic mutual coupling between different ferroic orders at room temperature are scarce and, so far, the attained magnetoelectric coupling strength is not sufficiently high to integrate them into real devices.[12,13] Artificial multiferroics, on the other hand, are ferromagnetic–ferroelectric heterostructures (which also exhibit magnetostrictive–piezoelectric coupled properties), where the coupling between the ferroelectric and ferromagnetic counterparts occurs extrinsically through strain-mediated magnetoelectric effects. An electric field generates a macroscopic strain in the ferroelectric material which is then transferred to the adjacent ferromagnetic material to modify its properties.[14–17] However, the required circuitry to apply electric fields hinders technological advances in this area because efficient and non-invasive control methods are often required for next-generation nanoelectronic devices.

Interestingly, it has been recently demonstrated that a reversible control of macroscopic polarization in $BaTiO_3$ (BTO) crystals using low-intensity visible light is possible.[18] Subsequent investigations have proven that this new concept of light–matter coupling delivers new paradigms for photo-controlled device development.[19–21] Undoubtedly, the non-contact external control of strain in ferroelectrics opens up a

[a]*Departament de Física, Universitat Politècnica de Catalunya, 08034 Barcelona, Spain. E-mail: jose.eduardo.garcia@upc.edu*
[b]*Departament de Física, Universitat Autónoma de Barcelona, 08193 Bellaterra, Spain. E-mail: jordi.sort@uab.cat*
[c]*Department of Electroceramics, Instituto de Cerámica y Vidrio – CSIC, 28049 Madrid, Spain. E-mail: frmarcos@icv.csic.es*
[d]*Institut de Ciència de Materials de Barcelona – CSIC, 08193 Bellaterra, Spain*
[e]*Institució Catalana de Recerca i Estudis Avançats (ICREA), 08010 Barcelona, Spain*
†Electronic supplementary information (ESI) available. See DOI: https://doi.org/10.1039/d3nr05520e
‡These authors contributed equally to this work.

vast range of opportunities. In particular, visible light may be used as an external actuation method to reversibly tune magnetic properties in artificial multiferroics. This concept has recently been used to manipulate the magnetic properties of a 40 nm-thick metallic nickel film grown onto a BTO crystal by the motion of ferroelectric domain walls *via* visible light illumination in a wide temperature range, from very low temperature up to close to room temperature.[5] However, no change in magnetization was detected at room temperature, thus hindering this effect from being translated into immediate applications. It is important to point out that heterostructures combining photostrictive and magnetostrictive constituents have already been explored by synthetizing heteroepitaxial self-assembled oxide nanostructures, showing, for instance, a light-induced ultrafast magnetization change of $CoFe_2O_4$ nanopillars embedded in a $SrRuO_3$ matrix.[22]

In this work, the non-contact external control of strain in a BTO crystal utilizing low-intensity visible light is used as a method to manipulate the magnetic easy axis and coercivity of magnetostrictive $Fe_{75}Al_{25}$ films in a reversible manner. $Fe_{75}Al_{25}$ was selected because of its high magnetostriction and previously reported magnetoelectric effects.[23] Giant and reversible visible-light-induced changes of magnetic properties are achieved in this heterostructure through a strain-mediated converse magneto-optical effect, at room temperature.

Experimental

Samples preparation

Two $BaTiO_3$ (BTO) single crystals were produced by top–seeded solution growth (TSSG). One of them was grown with (001) orientation and provided by SurfaceNet GmbH (Germany) while the other one was grown with (100) orientation and provided by PI-KEM Ltd (UK). Both 5 mm × 5 mm × 0.5 mm crystals were one-side polished and no further thermal and/or chemical etching was used to reveal the domain structure. 50 nm-thick $Fe_{75}Al_{25}$ (at%) films were grown by co-sputtering at room temperature on the polished face of both BTO single crystals using an AJA International, Inc. magnetron sputtering system, shaping the $Fe_{75}Al_{25}/BaTiO_3$ heterostructures. For sake of comparison, 50 nm-thick $Fe_{75}Al_{25}$ was also grown onto Si and $Pb(Mg_{1/3}Nb_{2/3})O_3$-32$PbTiO_3$ substrates.

Domain structure characterization

The domain mappings were performed using a confocal Raman microscope (Witec alpha-300R). Raman spectra were collected using a 532 nm excitation laser and a 100× objective lens. The lateral and vertical resolutions of the confocal microscope were 250 nm and 500 nm, respectively, with a spectral resolution of the Raman mode of 0.02 cm^{-1}. Under the microscope objective, the domain walls of the samples were adjusted perpendicular to the x axis and parallel to the y axis of the piezo-driven scan table. The light was focused onto the sample surface, with the light polarization parallel to the surface, and the scan direction (indicated as the x axis) was kept perpendicular to the a–c domain walls. The domain structure of the sample was controlled by capturing sequential depth scans. Accumulated Raman spectra were analysed using Witec Control Plus Software.

Microscopic strain characterization

The in-plane light-induced local deformation was measured using atomic force microscopy (AFM), which is coupled to the confocal Raman microscope (Witec alpha-300R). Topographic images of 30 μm × 30 μm lateral size were obtained in non-contact mode by scanning 256 lines with 512 points each at a frequency of 1 Hz. A custom setup coupled to AFM was used to carry out the experiments involving illumination. A laser diode (Thorlabs, Inc.) operating at a wavelength of 532 nm was used as light source. The procedure started with the AFM scanning the sample surface in dark condition. Then, after one-third of the total scanning was completed, the iris of the optical setup was opened, and the second third of the image was recorded. Finally, when the second third of the scanning is completed, the iris was closed and the last third of the image is recorded. The AFM images were taken with the Witec Control Plus Software and then were processed with MATLAB (The MathWorks, Inc.).

Macroscopic strain measurement

Light-induced deformation was measured using a WayCon inductive position transducer conditioning with a Solartron OD5 Module. The system has a linear scale of 42 V mm^{-1}, allowing measuring tens of nanometres using a high-resolution oscilloscope (Keysight DSOX2004A). For measurements under illumination conditions, a 532 nm wavelength laser diode (Thorlabs, Inc.) was coupled to the system. The power of the light source was controlled by a source measured unit (Keithley 2400) and was set to 50 mW. The light spot was adjusted at ∼2 mm in diameter and the light irradiation time was controlled using a switch. The data processing of the raw data allowed the elimination of the slow thermal drift. A Savitzky–Golay filter was used for smoothing the data.

Magnetic characterization

Room temperature magnetic properties were characterized with and without illumination using a MicroSense vibrating sample magnetometer from Quantum Design. The measurements were performed in the plane of the films while rotating the sample, to investigate in-plane magnetic anisotropy. The magnetometer is open and allows for a direct sample actuation with light. The 532 nm wavelength laser light was orthogonally directed towards the samples with a light spot of ∼2 mm in diameter.

Synchrotron radiation high-resolution X-ray diffraction

Measurements were carried out at the SpLine CRG BM25 beamline at the ESRF The European Synchrotron (Grenoble, France). The X-ray beam wavelength was set to 0.8266 Å (≈15 keV) with an energy resolution of $\Delta E/E \approx 10^{-4}$. The beam spot size was adjusted at 0.5 mm × 0.5 mm to ensure a representative measure of the domain structure of the crystal. Instrument calibration and wavelength refinement were performed with a

Lanthanum hexaboride (LaB_6) standard. Measurements were carried out in reflection geometry using a six-circle diffractometer in vertical configuration. The XRD patterns were recorded over the angular range 9°–40° (2θ) with a step size of 0.0075° using a 2D photon-counting X-ray MAXIPIX detector. Reciprocal space maps were measured, considering BTO lattice parameter units. All XRD data were processed with the BINoculars software. For measurements in illumination conditions, a 532 nm wavelength laser diode (Thorlabs, Inc.) was coupled to the measurement stage. The power of the light was set to 50 mW and the light spot was adjusted at of ~2 mm in diameter. The light irradiation time was controlled using an electronic switch.

Results and discussion

A highly homogenous 50 nm-thick $Fe_{75}Al_{25}$ (at%) thin film was grown on a highly oriented (001)-BTO crystal with engineered domain structure (Fig. 1a and b). An oriented array of in-plane and out-of-plane domains is evidenced (Fig. 1c and d) with a remarkable prevalence of out-of-plane domains, as verified by high-resolution synchrotron X-ray diffraction (Fig. 1e–g). The integrated intensity of the 002 peak is proportional to the number of ferroelectric domains that are perpendicular to the film plane, *i.e.*, out-of-plane domains, labelled as c-domains. Meanwhile, the number of in-plane, a-domains, is proportional to the integrated intensity of the 200 peak.

The visible-light-induced deformation of the FeAl/BTO heterostructure is explored as a first step to evidence that a strain-mediated light-control of magnetic properties is possible in this engineered magnetostrictive-ferroelectric heterostructure. Since the light-induced macroscopic strain in BTO originates mainly from the light-driven motion of the domain walls,[18,24] an anisotropic strain should be expected. Results show a significant macroscopic elongation of ~270 nm in the direction perpendicular to the domain walls arrangement upon light illumination (Fig. 2a) while a contraction of

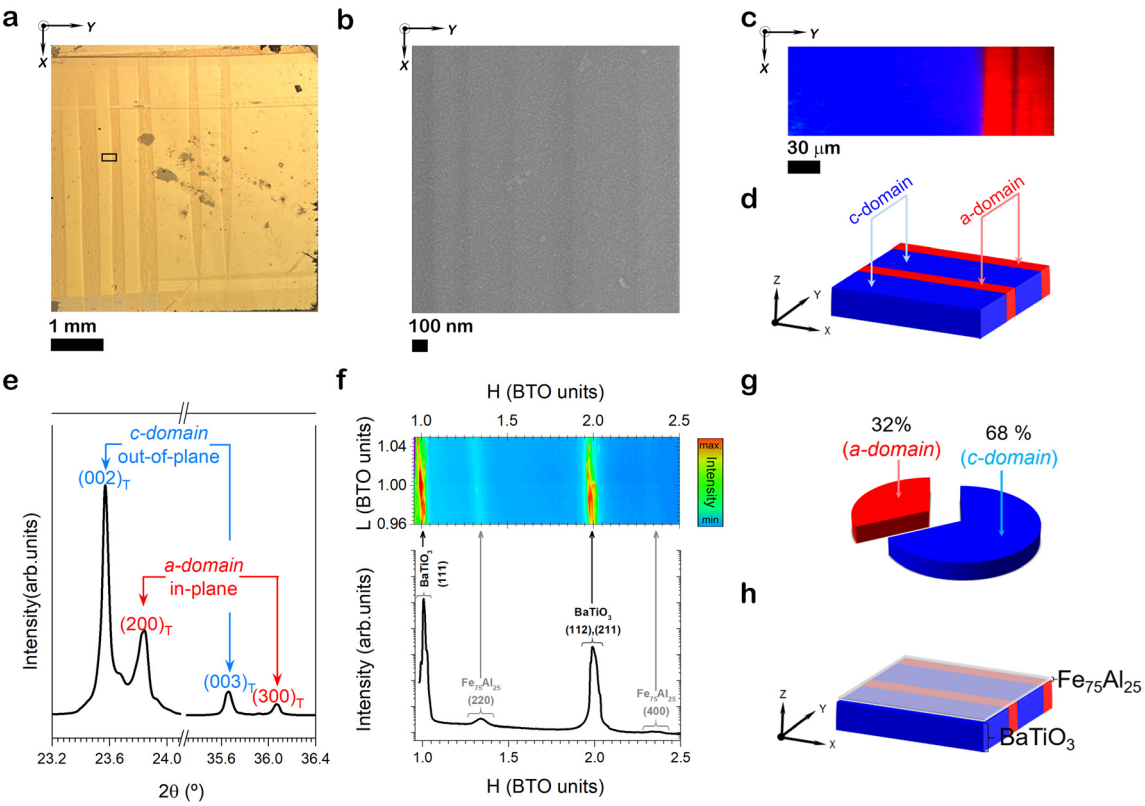

Fig. 1 Basic characterization of the $Fe_{75}Al_{25}/BaTiO_3$ artificial multiferroic. (a) Optical image of the sample surface showing differentiated, mostly parallel zones corresponding to domains with different polar orientations. Some irregular spots can be seen that were formed by handling the sample. (b) Scanning electron microscopy image taken using secondary electrons of the sample surface. A highly homogeneous $Fe_{75}Al_{25}$ film with strong degree of in-plane polycrystallinity is revealed. (c) Domain mapping corresponding to the area marked off by a black rectangle in panel (a). The Raman image resulted from the collected single depth-scan Raman spectra of each pixel of the rectangular area. Raman spectra with the same spectral shift for the Raman modes are identified using the same colour; that is, red for a-domains (in-plane) and blue for c-domain (out-of-plane). The intensity of the colour is correlated with the Raman intensity. (d) Schematic representation of the $BaTiO_3$ domain pattern showing a c–a-domain array. (e) X-ray diffraction pattern corresponding to the 200 and 300 reflections of the $BaTiO_3$. A dominant out-of-plane orientation of the crystal is evidenced. (f) Representative reciprocal space map along (H 0 1) planes (BTO units), and its H linear projection, where (220) and (400) $Fe_{75}Al_{25}$ are observed. (g) Domains distribution roughly estimated from the X-ray diffraction pattern. (h) Schematic representation of the $Fe_{75}Al_{25}/BaTiO_3$ heterostructure.

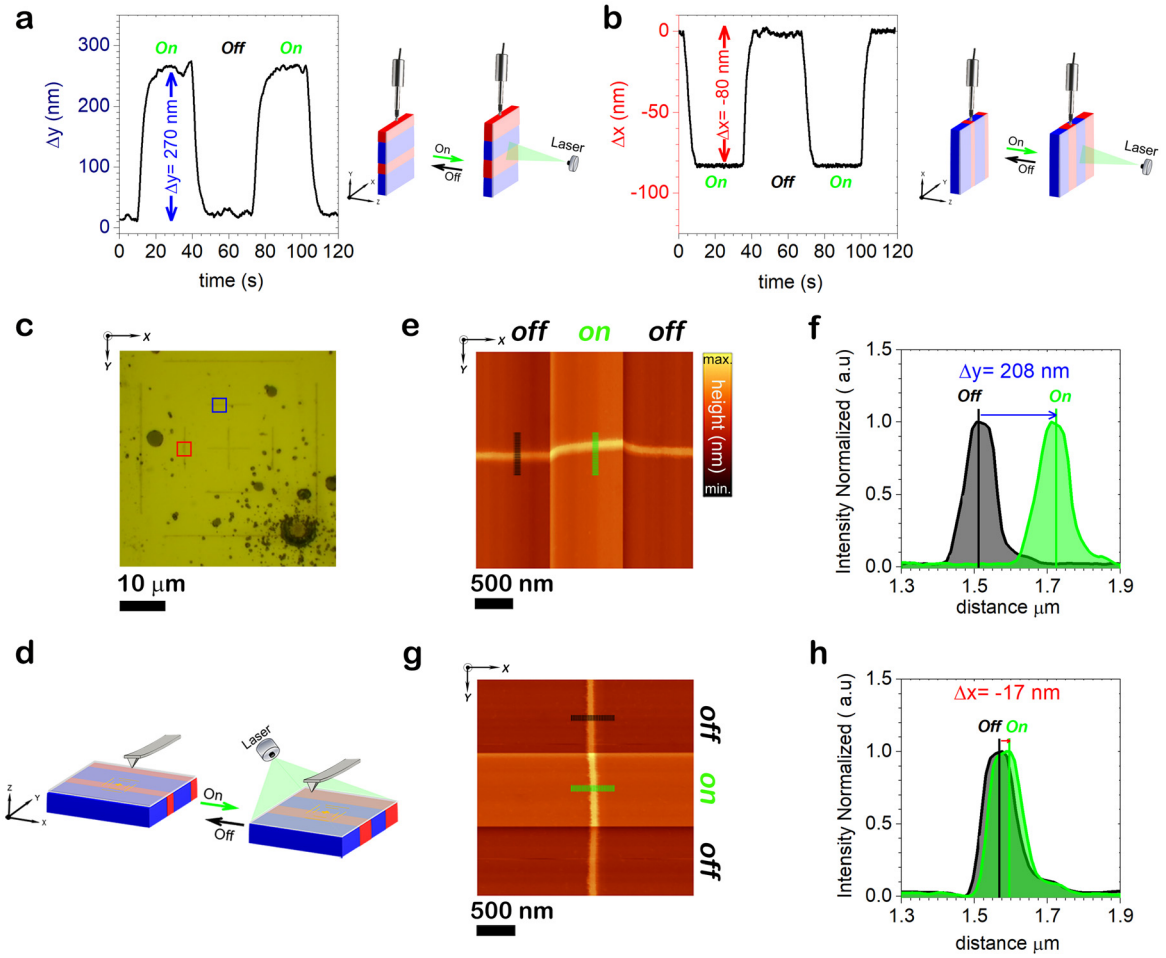

Fig. 2 Macro and microscopic photo-response of the $Fe_{75}Al_{25}/BaTiO_3$ artificial multiferroic. (a and b) Light-induced macroscopic deformation of the sample in the direction perpendicular (panel a) and parallel to the $BaTiO_3$ domain stripes (panel b). A significant elongation is photo-induced in the direction perpendicular to the domain walls while a slight contraction is revealed in the direction parallel to domain walls. Two cycles of light on–off were performed in order to ensure measurement repeatability. A measurement scheme is shown above the plots. (c) High-resolution optical image of a selected area of the sample surface. An arrangement of gold lines patterned by lithography is shown. Note that *y*-direction in this panel corresponds to *y*-direction in Fig. 1a. (d) Schematic illustration of the local measurement of the in-plane photo-deformation. (e) AFM topographic image displaying a sequential scan for a set composed of off–on–off illumination cycle for the region marked off with a blue square in panel (c). (f) Position of the gold line before and after illumination. The plotted profiles correspond with the drawn lines in the topographic image of panel (e). Data were extracted from the set of AFM profiles forming the whole image. (g) AFM topographic image displaying a sequential scan for a set composed of off–on–off illumination cycle for the region marked off with a red square in panel (c). (h) Position of the gold line before and after illumination. The plotted profiles correspond with the drawn lines in the topographic image of panel (e).

~80 nm is found in the direction parallel to the domain walls (Fig. 2b), thereby revealing a high anisotropic light-induced strain. Note that the elongation-contraction in orthogonal directions constitutes an irrefutable proof that the light-induced phenomenon is not temperature related, as mentioned in previous works.[18–20] For comparison purposes, a FeAl/BTO heterostructure with a macroscopically almost isotropic orientation of in-plane ferroelectric domain walls was also prepared (Fig. S1, ESI†). The same measurements show elongations of ~100 nm and ~60 nm in perpendicular directions. While the local deformations are partially compensated in an isotropic ferroelectric domain wall arrangement, a large anisotropic light-induced strain is obtained when domain walls are effectively anisotropically oriented. Atomic force microscopy imaging reveals that the $Fe_{75}Al_{25}$ thin film follows the same substrate elongation-contraction trend as the BTO crystal (Fig. 2e–h), evidencing an adequate matching between both materials. It is important to note that the attained elongation linearly depends on the light power (Fig. S2, ESI†), which represents a great advantage from the technological point of view.

Considering that there are piezoelectric materials with higher electric-field-induced deformation response than BTO, a 50 nm-thick $Fe_{75}Al_{25}$ (at%) thin film was also grown on top of a (110)-oriented $Pb(Mg_{1/3}Nb_{2/3})O_3$-32$PbTiO_3$ ferroelectric crystal, giving rise to a $Fe_{75}Al_{25}$/(PMN-PT) heterostructure. No macroscopic response could be induced by visible light in this artificial multiferroic, evidencing that both electric-field and

visible-light induced strain phenomena are not necessarily interrelated. Furthermore, the photovoltaic effect can be discarded as a primary mechanism for the visible-light-induced strain. It is well-known that PMN-PT exhibits photostriction when it is illuminated with UV light as a result of a converse piezoresponse induced by the photovoltage engendered by the bulk photovoltaic effect.[3,4]

Two crucial facts should be taken into account: (i) although piezoelectric materials have large mechanical response to electric fields, the visible-light-driven deformation will not be activated if they do not have an appropriate domain structure containing charged domain walls; (ii) even in ferroelectrics with charged domain walls, large light-driven anisotropic deformation is obtained only when an adequate domain configuration is designed. As hypothesis, other ferroelectric materials exhibiting stripe-shaped charged domain walls may manifest visible-light-induced strain.

Fig. 3 shows the magnetic response of the FeAl/BTO heterostructure with a highly anisotropic ferroelectric domain orientation, before and after illumination. The topography of the BTO substrate becomes imprinted to the FeAl layer, which acquire the stripe-like morphology of the underlying ferroelectric domains array, in a similar manner to what was reported for $CoFe/BaTiO_3$ and $Fe/BaTiO_3$ heterostructures.[25–27] Note that, reversibly controlled morphological changes at the surface of a ferromagnetic film has been proved to yield reproducible modifications of the ferromagnetic response of a multiferroic heterostructure.[28] Hence, in-plane hysteresis loops were taken while applying the magnetic field along (0°), diagonally (45°) and perpendicularly (90°) to the FeAl stripes to investigate magnetic anisotropy (Fig. 3a). Fig. 3b reveals a pronounced magnetic anisotropy, being the directions parallel (0°) and perpendicular (90°) to the stripes the easy and hard magnetic axes, respectively, governed by the shape anisotropy of the FeAl stripes. In contrast to the hysteresis loop acquired across the lines (90°), the measurement along the lines (0°) exhibits a double-step hysteresis loop. This is probably the result of dipolar interactions among FeAl stripes with dissimilar coercivity,[28,29] that stem from the slight growth differences and the sizes of the FeAl stripes, imposed by the ferroelectric domain pattern of the substrate beneath. In fact, the amount of magnetization drop at both coercivities is an indirect measure of the number of domains of each type. Since c-domains are predominant and the largest magnetization drop occurs for the harder magnetic phase, it is deduced that FeAl grown on c-domains exhibits larger coercivity than that grown-on a-domains. Hence, the magnetization of the FeAl grown on a-type domains will reverse prior to its counterpart for c-domains, anchoring its magnetization (Fig. 3c); that is, stabilizing the antiparallel alignment of the magnetizations,[29,30] and thus increasing the field needed to reverse the magnetization of the FeAl grown on c-type domains (becoming magnetically harder). Conversely, when applying the magnetic field perpendicularly to the stripes, once the magnetization of the FeAl grown on a-type domains is switched, this arrangement favours the magnetization reversal of the FeAl grown on c-type domains, resulting in the absence of magnetization reversal step (Fig. 3c). Fig. 3d–f show the hysteresis loops taken with and without illumination when the magnetic field is applied along (0°), diagonally (45°) and perpendicularly (90°) to the FeAl stripes, respectively. Optical actuation leads to a slight decrease in coercivity when magnetic hysteresis loops are measured along 0° and 45°, while keeping the remanent magnetization almost unaltered. Conversely, no appreciable changes in coercivity are observed along 90°. Nevertheless, there is a pronounced enhancement of the remanence (42% increase with respect to the pristine, non-illuminated, state), envisaging a change in magnetic anisotropy (specifically, from a hard to an easier magnetic behaviour). These effects can be ascribed to the strain arising from the BTO substrate upon illumination which is then transmitted to the FeAl film (*i.e.*, a strain-induced magnetic anisotropy).[31,32] As seen in Fig. 2, the FeAl/BTO heterostructure upon illumination undergoes a macroscopic elongation in the direction orthogonal to the domain walls (*i.e.*, across stripes, 90°) with a concomitant contraction in the direction parallel to the domain walls (*i.e.*, along stripes, 0°). This strain is transferred to the adjacent FeAl film, which undergoes inverse magnetostriction because of magnetoelastic coupling. The magnetoelastic coupling energy variation (ΔE_{mel}) undergone by a ferromagnet when subjected to a mechanical stress σ can be expressed as $\Delta E_{mel} = -\frac{3}{2}\lambda\sigma\cos^2(\theta)$, where λ is the magnetostriction constant of the ferromagnet and θ the angle between the direction of the applied stress and magnetization.[33] As seen in Fig. 2, a compressive stress arises along the lines (*i.e.*, $\sigma < 0$) when illuminating. Considering the magnetic easy axis lies along the lines and the magnetostriction constant of $Fe_{75}Al_{25}$ is positive,[34] the magnetoelastic coupling energy variation is minimized when θ = 90°, implying a reorientation/switch of the magnetic easy axis from the parallel to the perpendicular direction to the lines. Even though shape anisotropy rules the magnetic anisotropy in this system, magnetoelastic coupling arises, competing but not overcoming shape anisotropy upon illumination, resulting in a weaker magnetic anisotropy. The modulation of magnetic anisotropy by deformation can also be triggered by other means than light, such as phase transformation.[35]

Light intensity dependence was also explored by measuring the magnetic hysteresis loops along the lines (0°) at different light power, showing larger coercivity change for higher light power. Remarkably, the effect vanishes upon switching off the light, and the behaviour of the pristine state is recovered, indicating fully reversibility (Fig. S3, ESI†). Interestingly, when a similar FeAl/BTO heterostructure but with a nearly isotropic domain wall structure is considered, the optical modulation of magnetism is much weaker (ESI, section 1†) since local deformations are partially compensated, resulting in an isotropic light-induced strain with negligible generation of a well-defined strain-induced magnetic anisotropy. To rule out the possible heating effects in this optical modulation of magnetism, the FeAl film was also grown atop a 300 nm SiO_2/0.5 mm [100]-oriented Si substrate. In this case, the hysteresis loops

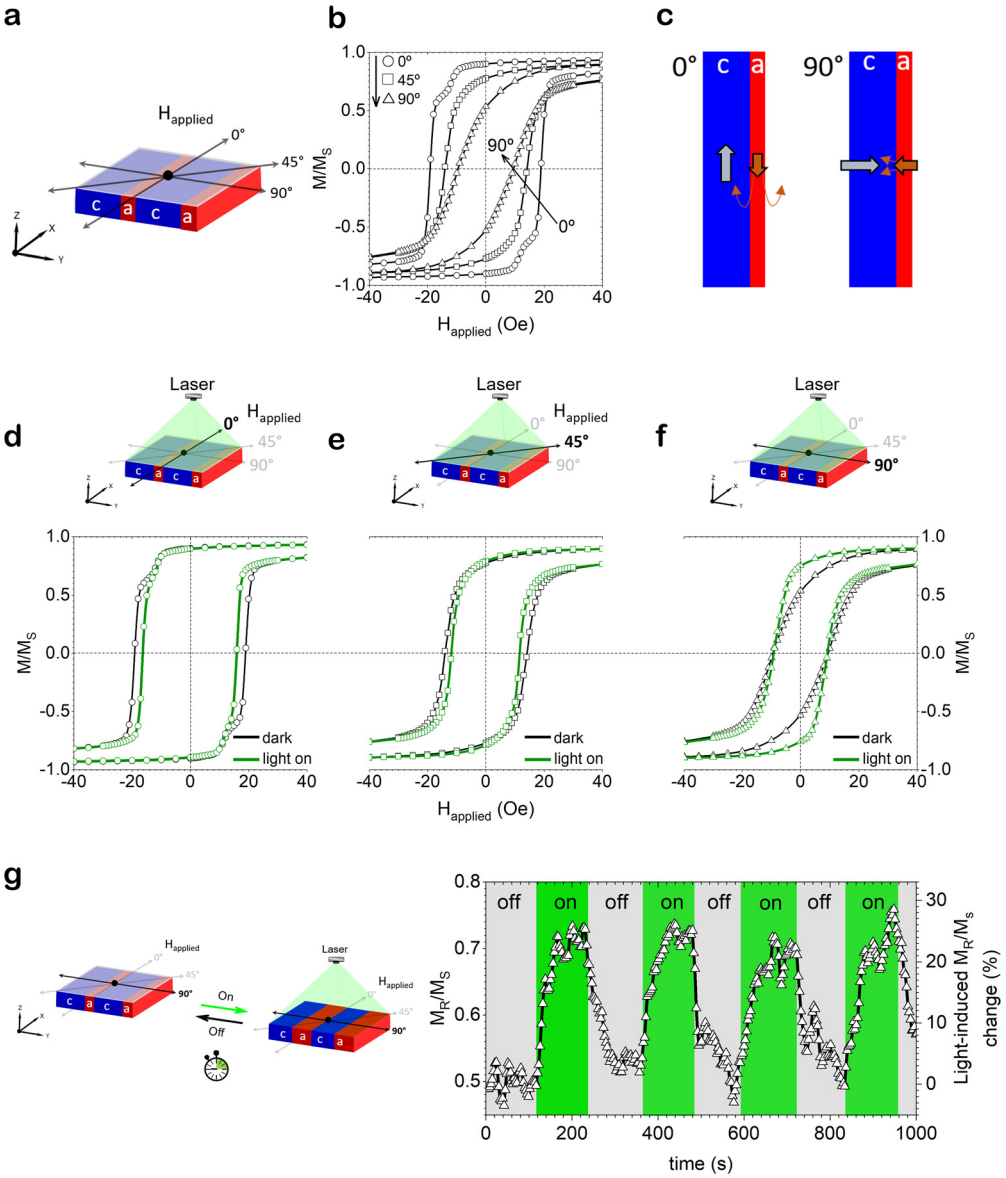

Fig. 3 Magnetic characterization of the FeAl/BTO artificial multiferroic before and after illumination. (a) Ferroelectric domain distribution with the used angular nomenclature for angular dependence characterization of magnetic properties. (b) Magnetic hysteresis loops (taken as remanent magnetization normalized to saturation magnetization M/M_S *versus* applied magnetic field $H_{applied}$) acquired without illumination along (0°), diagonally (45°) and perpendicularly (90°) to the stripes. (c) Effect of dipolar magnetic interactions among contiguous FeAl stripes when the magnetic field is applied along (on the left) and across (on the right) the lines. Arrows arising from FeAl stripes on a-domains represent magnetic stray fields. (d–f) Hysteresis loops before and after illumination (50 mW of light power) taken along (0°), diagonally (45°) and perpendicularly (90°) to the stripes, respectively. (g) Temporal sequence of light off–on experiments showing cyclability at remanence upon saturating the magnetic field perpendicularly (90°) to the FeAl stripes. The squareness (*i.e.*, the relation between remanent, M_R, and saturation, M_S, magnetizations) is plotted as a function of time. The percentage of the light-induced squareness change is also shown.

before and after illumination fully overlap (Fig. S4, ESI†), indicating that the observed optical modulation of magnetism is linked to inverse magnetostriction arising from the light-induced strain in BTO, as aforementioned. Moreover, no optical modulation is observed in the FeAl/PMN-PT heterostructure (Fig. S4, ESI†), reinforcing that visible-light- and electric-field-induced phenomena are not directly related. Finally, taking advantage of the reversibility of this optical modulation, cyclability induced by consecutive off–on illumination, at remanence, after saturating the magnetic field across the FeAl lines, is proven, showing the robust endurance of this effect (Fig. 3g). The remanent magnetization can be switched alternately between two states, the magnetization change being of ~20% for this experimental condition (Fig. 3g).

The light-driven domain wall motion has been postulated as the main mechanism for the control of strain in BTO.[21,24]

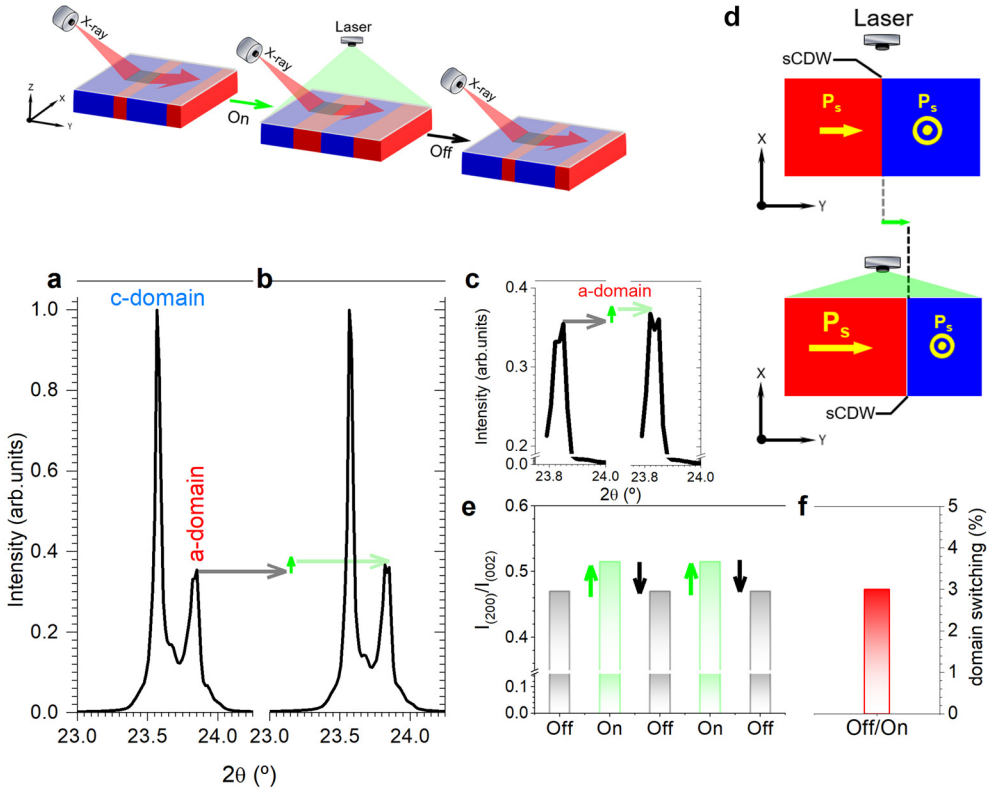

Fig. 4 Reversible optically-induced ferroelectric domain switching of $BaTiO_3$. (a and b) Synchrotron radiation high-resolution X-ray diffraction patterns of (002)/(200) reflections before and after illumination. The in-plane (a-domains) contribution enhances when the light is on as a result of the light-induced domain wall motion, as outlined above the plots. (c) Zoom of a-domains contribution before and after illumination. (d) Simplified scheme for the light-induced domain wall motion because of the illumination process. (e) Sequence of the relative integrated intensity of the (002) and (200) peaks, I_{002}/I_{200} ratio, corresponding to the off–on–off light succession. (f) Bar plot showing the estimate value of the percentage of the light-induce domain switching of $BaTiO_3$.

In the particular case of the here studied FeAl/BTO heterostructure, the highly oriented domain structure of BTO gives rise to a strong anisotropic strain (Fig. 2a and b) that is responsible for optical modulation of the magnetic properties of the $Fe_{75}Al_{25}$ film. The ON/OFF states of magnetization are achieved after a dynamic process that takes several second (Fig. 3g), according with the domain structure rearrangement in the BTO. Faster light-driven processes of domain manipulation have been recently reported, such as the optical reconfiguration of ferroelectric domains in bismuth ferrite.[36,37]

The effect of the illumination on the XRD pattern of BTO is analysed to provide evidence for the ferroelectric domain switching. Fig. 4a and b shows the light off-on influence on the relative intensity of the (200) and (002) peaks, I_{200}/I_{002} ratio, whose value rises significantly under illumination. Therefore, light illumination triggers a relative increase of a-domains (Fig. 4c and e), caused by optically-driven domain wall motion.[24] The reversibility of the domain rearrangement is illustrated by sequential off–on light cycles (Fig. 4e), where a succession of experiments reveals that the XRD pattern exhibits only two profiles, which correspond to the off–on domain configurations. A simplified calculation based on the XRD measurements shows that a light-driven c- to a-domain switching of *ca.* 3% is induced under the specific conditions of the performed XRD experiments.

Conclusion

An unprecedented reversible modulation of magnetism in $Fe_{75}Al_{25}/BaTiO_3$ heterostructures using low-intensity visible-light at room temperature is demonstrated, which is enabled by the existence of highly oriented electrically charged domain walls in $BaTiO_3$ arranged in arrays of alternating in-plane and out-of-plane ferroelectric stripe domains. Light actuation yields a net compressive stress along the stripes' direction caused by ferroelectric domain switching, which leads to a 90-degree reorientation of the magnetic easy axis. As a result, important changes in the values of coercivity and squareness ratio of the hysteresis loops are observed, which can be modulated by varying the light intensity. These results open a new pathway to accomplish the long-awaited light-induced control of magnetic properties at room temperature, which will allow the development of low energy-consumption wireless microelectronic devices, with applicability in widespread technological areas such as artificial intelligence (AI) and the internet of things (IoT).

Author contributions

J. E. G. conceived the idea. E. M., J. S., and J. E. G. planned the research and experiments. E. M. and F. R.-M. prepared the samples. E. M., D. A. O., and Z. M. performed the magnetic characterization. A. D. C. and F. R.-M. carried out the Raman measurements and the microscopic strain characterization. D. A. O. and J. E. G. made the macroscopic strain measurements. J. L.-S., F. R.-M. and A. D. C performed the synchrotron XRD experiments. D. A. O. and E. M. wrote the manuscript draft with inputs from J. E. G., F. R.-M., and J. S. All authors contributed to the discussion and to the final version of the manuscript. The work was supervised by J. E. G., F. R.-M., and J. S.

Conflicts of interest

There are no conflicts to declare.

Acknowledgements

Financial support from the Spanish Ministry of Science and Innovation (MCIN/AEI/10.13039/501100011033), through the Severo Ochoa FUNFUTURE (CEX2019-000917-S), PID2020-112548RB-I00, PID2020-116844RB-C21, PID2019-107727RB-I00, PIE: 2021-60-E-030, PIE: 2010-6-OE-013, and PID2020-114192RB-C41 projects program, from Generalitat de Catalunya (2021 SGR 00804 and 2021 SGR 00651), the European Research Council (2021-ERC-Advanced 'REMINDS' Grant No. 101054687) and MCIN/AEI/10.13039/501100011033 & "European Union NextGenerationEU/PRTR" (Grant CNS2022-135230) is acknowledged. We also acknowledge projects TED2021-130453B-C21, TED2021-130453B-C22 and TED2021-130957B-C51, funded by the Spanish Ministry of Science and Innovation (MCIN/AEI/10.13039/50110001103). E. M. is a Serra-Húnter fellow. F. R.-M. is indebted to Comunidad de Madrid for the financial support through the Doctorados Industriales project (IND2020/IND-17375), which is co-financed by the European Social Fund. J. L.-S. acknowledges the financial support from MCIN for the "Ramón y Cajal" contract RYC2022-035912-I, funded by the European Social Fund Plus. The authors also acknowledge the provision of the SpLine CRG BM25 beamline under the project MA-5601 at the European Synchrotron Radiation Facility (ESRF). Dr Juan Rubio-Zuazo and Mr Carlos Beltrán-Hernando are acknowledged for their assistance with the synchrotron XRD measurements.

References

1 B. Kundys, C. Meny, M. R. J. Gibbs, V. Da Costa, M. Viret, M. Acosta, D. Colson and B. Doudin, *Appl. Phys. Lett.*, 2012, **100**, 262411.
2 V. Iurchuk, D. Schick, J. Bran, D. Colson, A. Forget, D. Halley, A. Koc, M. Reinhardt, C. Kwamen, N. A. Morley, M. Bargheer, M. Viret, R. Gumeniuk, G. Schmerber, B. Doudin and B. Kundys, *Phys. Rev. Lett.*, 2016, **117**, 107403.
3 X. Zhang, X. Guo, B. Cui, J. Yun, J. Mao, Y. Zuo and L. Xi, *Appl. Phys. Lett.*, 2020, **116**, 132405.
4 D. Dagur, V. Polewczyk, A. Y. Petrov, P. Carrara, M. Brioschi, S. Fiori, R. Cucini, G. Rossi, G. Panaccione, P. Torelli and G. Vinai, *Adv. Mater. Interfaces*, 2022, **9**, 2201337.
5 A. Bagri, A. Jana, G. Panchal, S. Chowdhury, R. Raj, M. Kumar, M. Gupta, V. R. Reddy, D. M. Phase and R. J. Choudhary, *ACS Appl. Mater. Interfaces*, 2023, **15**, 18391.
6 A. Bagri, D. M. Phase and R. J. Choudhary, *Acta Mater.*, 2023, **255**, 119091.
7 M. Fiebig, T. Lottermoser, D. Meier and T. Morgan, *Nat. Rev. Mater.*, 2016, **1**, 16046.
8 Y. L. W. van Hees, P. van de Meugheuvel, B. Koopmans and R. Lavrijsen, *Nat. Commun.*, 2020, **11**, 3835.
9 C. Song, B. Cui, F. Li, X. Zhou and F. Pan, *Prog. Mater. Sci.*, 2017, **87**, 33.
10 N. Spaldin and R. Ramesh, *Nat. Mater.*, 2019, **18**, 203.
11 N. A. Hill, *J. Phys. Chem. B*, 2000, **104**, 6694.
12 W. Eerenstein, N. D. Mathur and J. F. Scott, *Nature*, 2006, **442**, 759.
13 R. Ramesh and N. A. Spaldin, *Nat. Mater.*, 2007, **6**, 21.
14 S. Geprägs, M. Opel, S. T. B. Goennenwein and R. Gross, *Phys. Rev. B: Condens. Matter Mater. Phys.*, 2012, **86**, 134432.
15 T. H. E. Lahtinen, K. J. A. Franke and S. van Dijken, *Sci. Rep.*, 2012, **2**, 258.
16 S. Geprägs, D. Mannix, M. Opel, S. T. B. Goennenwein and R. Gross, *Phys. Rev. B: Condens. Matter Mater. Phys.*, 2013, **88**, 054412.
17 M. Ghidini, R. Pellicelli, J. L. Prieto, X. Moya, J. Soussi, J. Briscoe, S. Dunn and N. D. Mathur, *Nat. Commun.*, 2013, **4**, 1453.
18 F. Rubio-Marcos, D. A. Ochoa, A. Del Campo, M. A. García, G. R. Castro, J. F. Fernández and J. E. García, *Nat. Photonics*, 2018, **12**, 29.
19 D. Paez-Margarit, F. Rubio-Marcos, D. A. Ochoa, A. Del Campo, J. F. Fernández and J. E. García, *ACS Appl. Mater. Interfaces*, 2018, **10**, 21804.
20 F. Rubio-Marcos, D. Paez-Margarit, D. A. Ochoa, A. Del Campo, J. F. Fernández and J. E. García, *ACS Appl. Mater. Interfaces*, 2019, **11**, 13921.
21 V. Dwij, B. K. De, S. Rana, H. S. Kunwar, S. Yadav, S. R. Sahu, R. Venkatesh, N. P. Lalla, D. M. Phase, D. K. Shukla and V. G. Sathe, *Phys. Rev. B*, 2022, **105**, 134103.
22 H.-J. Liu, L.-Y. Chen, Q. He, C.-W. Liang, Y.-Z. Chen, Y.-S. Chien, Y.-H. Hsieh, S.-J. Lin, E. Arenholz, C.-W. Luo, Y.-L. Chueh, Y.-C. Chen and Y.-H. Chu, *ACS Nano*, 2012, **6**, 6952.
23 E. Menéndez, V. Sireus, A. Quintana, I. Fina, B. Casals, R. Cichelero, M. Kataja, M. Stengel, G. Herranz, G. Catalán, M. D. Baró, S. Suriñach and J. Sort, *Phys. Rev. Appl.*, 2019, **12**, 014041.

24 J. Ordoñez-Pimentel, M. Venet, D. A. Ochoa, F. Rubio-Marcos, J. F. Fernández and J. E. García, *Phys. Rev. B*, 2022, **106**, 224110.
25 T. H. E. Lahtinen, J. O. Tuomi and S. van Dijken, *IEEE Trans. Magn.*, 2011, **47**, 3768.
26 T. H. E. Lahtinen, J. O. Tuomi and S. van Dijken, *Adv. Mater.*, 2011, **23**, 3187.
27 T. H. E. Lahtinen, Y. Shirahata, L. Yao, K. J. A. Franke, G. Venkataiah, T. Taniyama and S. van Dijken, *Appl. Phys. Lett.*, 2012, **101**, 262405.
28 G. Vinai, F. Motti, V. Bonanni, A. Y. Petrov, S. Benedetti, C. Rinaldi, M. Stella, D. Cassese, S. Prato, M. Cantoni, G. Rossi, G. Panaccione and P. Torelli, *Adv. Electron. Mater.*, 2019, **5**, 1900150.
29 J. I. Martín, J. Nogués, K. Liu, J. L. Vicent and I. K. Schuller, *J. Magn. Magn. Mater.*, 2003, **256**, 449.
30 M. Varón, M. Beleggia, T. Kasama, R. J. Harrison, R. E. Dunin-Borkowski, V. F. Puntes and C. Frandsen, *Sci. Rep.*, 2013, **3**, 1234.
31 D. Sander, *Rep. Prog. Phys.*, 1999, **62**, 809.
32 D. Sander, *J. Phys.: Condens. Matter*, 2004, **16**, R603.
33 E. Trémolet de Lacheisserie, D. Gignoux and M. Schlenker, *Magnetism I – Fundamentals*, Kluwer Academic Publishers, Dordrecht, Netherland, 2002.
34 N. Mehmood, R. S. Turtelli, R. Grössinger and M. Kriegisch, *J. Magn. Magn. Mater.*, 2010, **322**, 1609.
35 A. Lisfi, C. M. Williams, L. T. Nguyen, J. C. Lodder, A. Coleman, H. Corcoran, A. Johnson, P. Chang, A. Kumar and W. Morgan, *Phys. Rev. B: Condens. Matter Mater. Phys.*, 2007, **76**, 054405.
36 Y.-D. Liou, Y.-Y. Chiu, R. T. Hart, C.-Y. Kuo, Y.-L. Huang, Y.-C. Wu, R. V. Chopdekar, H.-J. Liu, A. Tanaka, C.-T. Chen, C.-F. Chang, L. H. Tjeng, Y. Cao, V. Nagarajan, Y.-H. Chu, Y.-C. Chen and J.-C. Yang, *Nat. Mater.*, 2019, **18**, 580.
37 B. Guzelturk, T. Yang, Y.-C. Liu, C.-C. Wei, G. Orenstein, M. Trigo, T. Zhou, B. T. Diroll, M. V. Holt, H. Wen, L.-Q. Chen, J.-C. Yang and A. M. Lindenberg, *Adv. Mater.*, 2023, **35**, 2306029.